Characterization of living skin using multi-view stereo and isogeometric analysis

Adrián Buganza Tepole[a], Michael Gart[b], Arun K. Gosain[b], Ellen Kuhl[c]

[a]*Department of Mechanical Engineering, Stanford University, Stanford, CA 94305, USA*
[b]*Division of Pediatric Plastic Surgery, Lurie Children's Hospital of Northwestern University Feinberg School of Medicine, Chicago, IL 60611, USA*
[c]*Departments of Mechanical Engineering, Bioengineering, and Cardiothoracic Surgery, Stanford University, Stanford, CA 94305, USA,*
email: ekuhl@stanford.edu, phone: +1.650.450.0855, fax: +1.650.725.1587, URL: http:/biomechanics.stanford.edu, corresponding author

Abstract

Skin is our interface with the outside world. In its natural environment, it displays unique mechanical characteristics such as prestretch and growth. While there is a general agreement on the physiological importance of these features, they remain poorly characterized, mainly because they are difficult to access with standard laboratory techniques. Here we present a new, inexpensive technique to characterize living skin using multi-view stereo and isogeometric analysis. Based on easy-to-create hand-held camera images, we quantify prestretch, deformation, and growth in a controlled porcine model of chronic skin expansion. Over a period of five weeks, we gradually inflate an implanted tissue expander, take weekly photographs of the experimental scene, reconstruct the geometry from a tattooed surface grid, and create parametric representations of the skin surface. After five weeks of expansion, our method reveals an average area prestretch of 1.44, an average area stretch of 1.87, and an average area growth of 2.25. Area prestretch is maximal in the ventral region with 2.37, area stretch and area growth are maximal above the center of the expander with 4.05 and 4.81. Our study has immediate impact on understanding living skin to optimize treatment planning and decision making in plastic and reconstructive surgery. Beyond these direct implications, our experimental design has broad applications in clinical research and basic sciences: It serves as a simple, robust, low cost, easy-to-use tool to reconstruct living membranes, which are difficult to characterize in a conventional laboratory setup.

Keywords: Skin; prestretch; growth; multi-view stereo; isogeometric analysis

1. Motivation

Characterizing deformations under controlled ex vivo and natural in vivo conditions is key to understanding the mechanics of living membranes [28]. With a surface area of 2m^2, skin is the largest living membrane of our body. Healthy skin is vital to our existence: It protects, senses, regulates, and controls the biochemical, thermal, and mechanical interactions with our environment [33]. Four decades ago, pioneering experiments have characterized the ex vivo mechanics of explanted rabbit skin using uniaxial and biaxial testing [32, 53]. Other popular ex vivo setups for biological tissues include compression [8], shear [31], indentation [22], inflation [39], and bulge testing [54]. Recent attempts have focused on characterizing the mechanics of skin in vivo using either indentation [40] or aspiration [36]. Both are particularly valuable when combined with inverse finite element analyses [4]. Yet, with most conventional test setups, characterizing living membranes in vivo over long periods of time remains challenging. One possibility would be to label characteristic anatomic landmarks with implanted markers, follow them chronically, and reconstruct the surface geometry using biplane videofluoroscopy and continuum mechanics [41]. However, this approach is not only expensive and highly invasive, but also relies on a sophisticated, difficult-to-reproduce experimental setup.

Skin has two major advantages that distinguish it from many biological tissues: It is a thin membrane defined primarily through its surface representation [25], and it is conveniently exposed to facilitate surface imaging. Reconstructing skin surfaces from two-dimensional image capture is not a new idea; recent bulge experiments have used stereoscopic digital image correlation to identify the material parameters of explanted human skin samples [55]. Yet, these experiments require a restrictive laboratory setup and have so far only been used in ex vivo and acute conditions. Here, we propose an alternative, inexpensive, easy-to-use method for surface reconstruction of living surfaces in vivo: multi-view stereo. Multi-view stereo is a technique that allows us to extract three-dimensional representations of scenes from a collection of multiple two-dimensional images [46]. Reconstructing three-dimensional geometries has been one of the major challenges in computer graphics since the early seventies, but it is only within the past decade that multi-view stereo has rapidly evolved into a robust and reliable reconstruction tool [24, 35]. Initial stereo vision relied on sophisticated calibrations and precisely known camera positions [49]. The power of multi-view stereo has increased noticeably with the automatization of these calibrations allowing us to use random sets of photographs with arbitrary camera angles [51]. Not surprisingly, multi-view stereo is now finding its way into several commercial tools including the popular Cubify Capture

and Autodesk 123D Catch. The high accuracy of model reconstruction with errors of the order of 2% suggests that multi-view stereo can be used to reliably reconstruct triangulations of living surfaces in their natural in vivo environment [21].

To analyze the reconstructed three-dimensional scenes, it is critical to create parametric surface representations to quantify the relative deformation between points in space and time. A powerful computational approach for generating and analyzing free form surfaces is isogeometric analysis [14]. In contrast to conventional finite element analysis [26], isogeometric analysis employs B-spline basis function to represent both the geometry and the fields of interest [27]. Isogeometric analysis offers several advantages, which become particularly relevant when characterizing thin membranes [16]: B-spline basis functions enable the representation of smooth surfaces with only a few arbitrary control points [7]; their high polynomial degree inherently ensures high continuity, which is critical to characterize surface strain, surface curvature, and higher order derivatives [30]; and they allow us to use the same surface parametrization for different surfaces to easily quantify kinematic changes in both space and time.

Here, we are particularly interested in kinematic changes in time to characterize membrane growth [1]. Living membranes grow and remodel in response to mechanical cues [44]. When stretched beyond the physiological limit, skin increases its surface area to achieve mechanical homeostasis [15]. Plastic and reconstructive surgeons capitalize on this phenomenon with an in situ procedure known as skin expansion, which creates skin with the same color, texture, hair-bearing characteristics, and mechanical properties as the surrounding tissue [23]. Skin expansion is widely used to correct large birth defects, burn injuries, defects resulting from tumor excision, and breasts following mastectomy [34].

The clinical relevance of skin expansion has long drawn the attention of clinical scientists and researchers who have conducted various studies to investigate the biological, biochemical, biomechanical, and physical changes in expanded skin [3]. As a result, our understanding of the mechanobiology of the dermis has largely improved [12, 48]; yet, several important aspects are still understudied and require ongoing research efforts [9, 13]. Perhaps the most crucial limitation of skin expansion is the lack of a quantitative mechanistic understanding of the interplay between reversible elastic deformation and permanent area growth [56]. This limits the use of the procedure to senior and very experienced surgeons [47].

Chronically expanded skin grows primarily in the plane, while its thickness remains virtually unchanged [6]. Continuum models for skin growth represent this effect by decomposing the deformation gradient into an elastic part and a growth part [45]. For skin, the growth part is a transversely isotropic second order tensor parameterized in a single scalar-valued variable, the in-plane area growth [10]. We have demonstrated that area growth models can qualitatively predict skin growth for different tissue expander shapes [11] and for different patient specific geometries [58]. However, to serve as a quantitative predictive clinical tool, the model needs further experimental calibration and validation [59]. This is the main motivation for the present work.

2. Methods

2.1. Animal model

We select Yucatan domestic miniature swine (Sinclair Bio Resources LCC, Columbia, Missouri) as animal model for skin expansion. The white lineage of these swine is purpose-bred, hairless, and ideally suited for dermal studies. The anatomy and mechanical properties of porcine skin closely resembles those of human skin [37, 38]. Porcine models of wound healing agreed to 78% with human studies, while small animal models and in vitro studies only displayed an agreement of 53% and 57% [52]. The absence of redundant skin and a panniculus carnosus layer makes pigs a preferred model system whose structure closely resembles human conditions [5].

2.1.1. Surgical procedure

We acclimate a one-month-old male Yucatan miniature swine to standard housing and feed it ad libitum under a protocol approved by the Ann & Robert H. Lurie Children's Hospital of Chicago Research Center Animal Care and Use Committee.

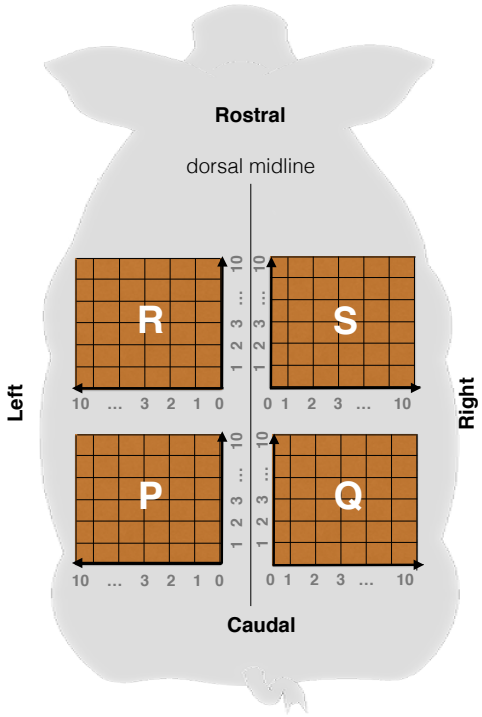

Figure 1: Porcine model for skin expansion. Four zones are identified by 10 cm × 10 cm grids tattooed on the pig's back in the left caudal (P), right caudal (Q), left rostral (R), and right rostral (S) regions. Rectangular tissue expanders are placed beneath the left caudal (P) and right rostral (S) regions; the right caudal (Q) and left rostral (S) regions serve as controls.

On the day of surgery, we administer pre-procedural antibiotics and clean the dorsal skin with chlorhexidine-based surgical soap. We transfer 10 cm × 10 cm grids with 1cm line markings to the pig's skin using tattoo transfer medium in four areas, left caudal (P), right caudal (Q), left rostral (R), and right rostral (S), as illustrated in Figure 1. Our template contains a midline reference to ensure symmetric placement of the grid patterns.

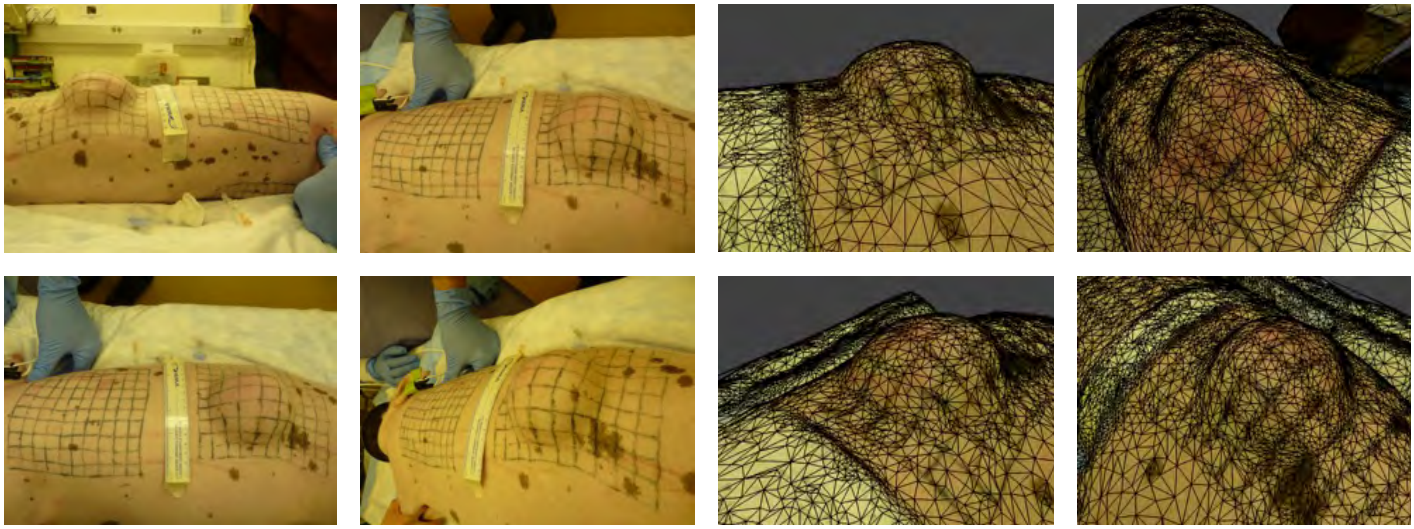

Figure 2: Multi-view stereo is a technique to extract three-dimensional representations of scenes from a collection of multiple two-dimensional images. Selected photographs from different camera angles show the experimental setup with the tattooed grid and the inflated tissue expander in the left caudal region, left. Similar views show the reconstructed triangular surface representation of the scene created using online multi-view stereo, right.

The grids are permanently tattooed onto the pig's skin using a commercially available tattoo machine.

We record measurements and take photographs of the experimental setup before expander implantation. Then we inject local anesthetic (1% lidocaine with 1 : 100000 epinephrine) subcutaneously at the site of each planned incision. We place two 120 cc textured, rectangular tissue expanders of dimensions 4 cm × 6 cm (PMT Corporation, Chanhassen, MN) beneath the left caudal (P) and right rostral (S) tattooed grid. Each expansion site has a mirror image grid of non-expanded tissue, (Q) and (R), as an internal control for prestretch and growth. A subcutaneous filling port near the dorsal midline, outside of the measurement grid, connects to each expander and allows for controlled inflation.

We close the incisions in standard fashion, and remove the sutures 14 days postoperatively. We monitor the animal postoperatively until it is able to maintain upright posture. We continue antibiotic prophylaxis for 48 hours (Combi-Pen-48, Bimeda, Inc., Dublin, Ireland), and buprenorphine (0.05-0.1mg/kg) for analgesia via intramuscular injection every 12 hours for 4 doses, with additional doses available for evidence of animal distress.

2.1.2. Skin expansion

We leave the incisions to heal for three weeks before beginning expansion. Weekly, we fill the right rostral expander (S) by 25 cc and the left causal expander (P) by 50 cc, for five consecutive expansions to total volumes of 125 cc and 250 cc. Following the fifth expansion, we let the tissues settle for five days before we perform a final small expansion of 15 cc and 30 cc three days before tissue harvest.

2.1.3. Tissue harvest and euthanasia

On the day of tissue harvest, we anesthetize the animal as described above and record final tissue measurements. We excise the four tattooed skin patches and euthanize the animal using intravenous overdose of pentobarbital (90mg/kg). We take photographs of the explanted tissues, fix them, and embed them in paraffin for subsequent analyses.

2.2. Multi-view stereo

Every week, before and after filling, we take ten photographs of the experimental scene from different camera angles. We reconstruct the three-dimensional geometry from these multiple two-dimensional images using online multi-view stereo (Autodesk 123D Catch, Autodesk Inc., San Rafael, California). To calibrate the lengths and quantify the error of the geometric reconstruction we include a ruler during photo acquisition.

Figure 2 shows four different views of the experimental setup, left, and similar views of the reconstructed triangular surface representation, right. To calibrate the lengths, for each set of images, we fit a cubic spline to the ruler and determine the individual lengths l_i along the spline between the $i = 1, .., n$ one-cm-long ruler segments. We scale the geometry between the acquired images and the physical world using the average length $l = \sum_{i=1}^{n} l_i \,/\, n$. To quantify the average geometric reconstruction error, we calculate the average error $e = \sum_{i=1}^{n} e_i \,/\, n$ as the average of the individual reconstruction errors of each segment, $e_i = [l_i - l] \,/\, l$.

2.3. Isogeometric surface representation

To create a functional surface representation of the skin patch, we fit a B-spline surfaces through the 11 × 11 tattooed nodes. B-spline surfaces are tensor products of B-spline curves. A B-spline curve $C(\xi)$ is the sum of a set of the basis functions $N_i(\xi)$ multiplied by the coordinates of a set of control points $\boldsymbol{P}_i$ summed over all $i = 1, .., n_{\mathrm{cp}}$ control points,

$$C(\xi) = \sum_{i=0}^{n_{\mathrm{cp}}} N_i(\xi)\, \boldsymbol{P}_i \,. \tag{1}$$

The B-spline basis functions $N_i(\xi)$ of degree p are associated with a knot vector $\boldsymbol{\Xi}$, a set of non-decreasing numbers $\boldsymbol{\Xi} = [\xi_0, \xi_1, ..., \xi_n]$, in which the first and last values, ξ_0 and ξ_n, are repeated p+1 times. The basis functions $N_i(\xi)$ follow a

recursive definition based on the zeroth order basis function for $p = 0$,

$$N_i^0(\xi) = \begin{cases} 0 & \xi_i \le \xi \le \xi_{i+1} \\ 1 & \text{otherwise}\,, \end{cases} \tag{2}$$

combined with the recursion equation for the higher order basis functions for $p \ge 1$,

$$N_i^p(\xi) = \frac{\xi - \xi_i}{\xi_{i+p} - \xi_i} N_i^{p-1}(\xi) + \frac{\xi_{i+p+1} - \xi}{\xi_{i+p+1} - \xi_{i+1}} N_{i+1}^{p-1}(\xi)\,. \tag{3}$$

A B-spline surface $\mathcal{S}(\xi,\eta)$ is the sum of a set of surface basis functions $N_i(\xi,\eta)$ multiplied by the coordinates of a set of control points $\boldsymbol{P}_i$ summed over all $i = 1,..,n_{\text{cp}}$ control points,

$$\mathcal{S}(\xi,\eta) = \textstyle\sum_{i=0}^{n_{\text{cp}}} N_i(\xi,\eta)\, \boldsymbol{P}_i\,. \tag{4}$$

The surface basis functions $N_i(\xi,\eta)$ are the tensor products of the B-spline basis functions $N_i(\xi)$ and $N_j(\eta)$ defined in equations (2) and (3). To approximate our tattooed grid, we choose B-spline basis functions of polynomial degree $p = 3$ based on a knot vector $\boldsymbol{\Xi} = [0,0,0,0,1,2,...,9,10,10,10,10]$. Using a best fit algorithm, we determine the sets of optimal control points $\boldsymbol{P}_i$ with

$$\textstyle\sum_{n=1}^{121} \| \boldsymbol{X}_n - \mathcal{S}_0(\xi,\eta) \| \to \min\,, \tag{5}$$

to characterize the surface $\mathcal{S}(\xi,\eta)$, which best approximates the $n = 1,..,11\times 11$ coordinates of the tattooed nodes.

2.4. Isogeometric analysis

Figure 3 illustrates two isogeometric surfaces reconstructed from our tattooed grid. To characterize the relative deformation between two points in time, we create two parametric surface representations of the skin patch, one at the reference state $\mathcal{S}_0$ and one at the current state $\mathcal{S}_t$.
Using the B-spline surfaces representation (4), we approximate the referential and current coordinates,

$$\begin{aligned} \boldsymbol{X} &= \textstyle\sum_{i=0}^{n_{\text{cp}}} N_i(\xi,\eta)\; \boldsymbol{P}_i \\ \boldsymbol{x} &= \textstyle\sum_{i=0}^{n_{\text{cp}}} N_i(\xi,\eta)\; \boldsymbol{p}_i\,, \end{aligned} \tag{6}$$

where $N_i(\xi,\eta)$ are the B-spline basis functions defined in equations (2) and (3) and $\boldsymbol{P}_i$ and $\boldsymbol{p}_i$ are the sets of optimal control points defined through the best fit (5). From the partial derivatives of the surface basis function with respect to the parametric coordinates, $N_{i,\xi}$ and $N_{i,\eta}$, we calculate the sets of covariant surface base vectors in the reference and current configurations,

$$\begin{aligned} \boldsymbol{G}_1 &= \textstyle\sum_{i=0}^{n_{\text{cp}}} N_{i,\xi}\; \boldsymbol{P}_i \qquad \boldsymbol{G}_2 = \textstyle\sum_{i=0}^{n_{\text{cp}}} N_{i,\eta}\; \boldsymbol{P}_i \\ \boldsymbol{g}_1 &= \textstyle\sum_{i=0}^{n_{\text{cp}}} N_{i,\xi}\; \boldsymbol{p}_i \qquad \boldsymbol{g}_2 = \textstyle\sum_{i=0}^{n_{\text{cp}}} N_{i,\eta}\; \boldsymbol{p}_i\,. \end{aligned} \tag{7}$$

To determine the contravariant base vectors $\boldsymbol{G}^\alpha$, we calculate the covariant surface metric,

$$G_{\alpha\beta} = \boldsymbol{G}_\alpha \cdot \boldsymbol{G}_\beta \quad \text{with} \quad \alpha,\beta = 1,2 \tag{8}$$

invert it to calculate the contravariant surface metric $G^{\alpha\beta}$, and map the covariant base vectors $\boldsymbol{G}_\beta$ onto their contravariant counterparts,

$$\boldsymbol{G}^\alpha = G^{\alpha\beta}\boldsymbol{G}_\beta \quad \text{with} \quad G^{\alpha\beta} = [\, G_{\alpha\beta}\,]^{-1}\,. \tag{9}$$

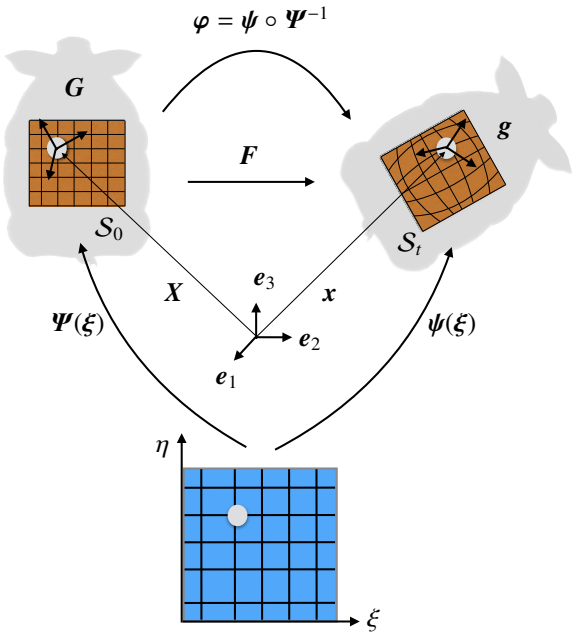

Figure 3: Isogeometric surfaces. The two mappings $\boldsymbol{\Psi}$ and $\boldsymbol{\psi}$ map the common parameter space (ξ,η) onto the reference and current surfaces $\mathcal{S}_0$ and $\mathcal{S}_t$. The deformation $\boldsymbol{\varphi} = \boldsymbol{\psi} \circ \boldsymbol{\Psi}^{-1}$ maps points between both surfaces as $\boldsymbol{x} = \boldsymbol{\varphi}(\boldsymbol{X})$. The deformation gradient $\boldsymbol{F} = \boldsymbol{g}_\alpha \otimes \boldsymbol{G}^\alpha$ is the key kinematic quantity to characterize pointwise relative deformation between the two surfaces.

Finally, we calculate the deformation gradient $\boldsymbol{F}$ as the dyadic product between the covariant current base vectors $\boldsymbol{g}_\alpha$ and the contravariant reference base vectors $\boldsymbol{G}^\alpha$,

$$\boldsymbol{F} = \boldsymbol{g}_\alpha \otimes \boldsymbol{G}^\alpha\,. \tag{10}$$

The deformation gradient is the key kinematic quantity to characterize the expansion process between any two time points across the tattooed grid. Its determinant characterizes the area stretch ϑ,

$$\vartheta = \det(\boldsymbol{F})\,, \tag{11}$$

the change in surface area between a surface element in the reference configuration $\mathcal{S}_0$ and in the current configuration $\mathcal{S}_t$.

2.5. Prestretch, expansion-induced deformation, and growth

Figure 4 illustrates the four distinct configurations of the skin patch to characterize prestretch, expansion-induced deformation, and growth. We define the explanted, stress free skin patch (Q) as the ex vivo pre-expansion configuration, which we map onto the in vivo pre-expansion configuration via the prestretch $\boldsymbol{F}^{\text{p}}$. This implies that the in vivo pre-expansion configuration is not necessarily stress-free; yet, it is convenient to choose it as a reference state since it coincides with the specific time point at the beginning of the experiment. We define the harvested, explanted skin patch (P) as the ex vivo grown patch, defined either through mapping the ex vivo pre-expansion patch with the growth tensor $\boldsymbol{F}^{\text{g}}$ or through the released elastic deformation $\boldsymbol{F}^{\text{e}\,-1}$ when compared with the in vivo expanded state. Figure 4 summarizes the relations between the total deformation gradient $\boldsymbol{F}$, the prestretch $\boldsymbol{F}^{\text{p}}$, the elastic tensor $\boldsymbol{F}^{\text{e}}$, and the growth

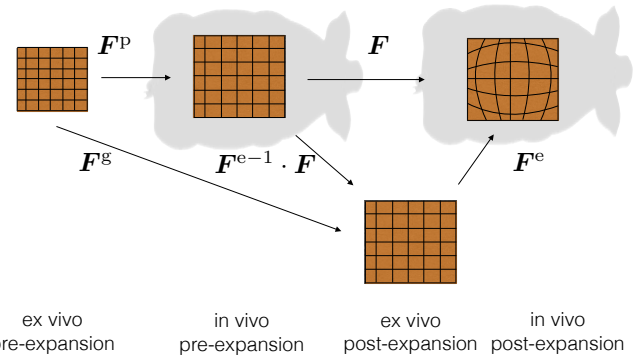

Figure 4: Four configurations of the skin patch: ex vivo pre-expansion, in vivo pre-expansion, ex vivo post-expansion, and in vivo post-expansion. The ex vivo pre-expansion patch can be mapped onto the in vivo post-expansion patch via prestretch $\boldsymbol{F}^{\mathrm{p}}$ and deformation $\boldsymbol{F}$, or, alternatively, via growth $\boldsymbol{F}^{\mathrm{g}}$ and elastic deformation $\boldsymbol{F}^{\mathrm{e}}$.

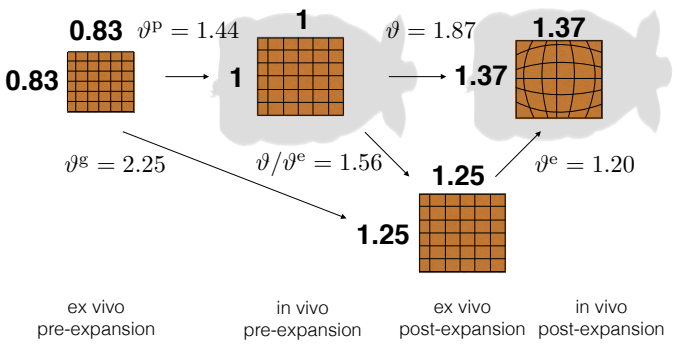

Figure 5: Four configurations of the skin patch. Prestretch induces an average area change of $\vartheta^{\mathrm{p}} = 1.44$. Expander inflation induces an average area change of $\vartheta = 1.87$, of which $\vartheta^{\mathrm{e}} = 1.20$ are reversible elastic and $\vartheta/\vartheta^{\mathrm{e}} = 1.56$ are permanently grown. When compared to the ex vivo pre-expansion skin patch, the ex vivo post-expansion patch has grown in area by $\vartheta^{\mathrm{g}} = 2.25$.

tensor $\boldsymbol{F}^{\mathrm{g}}$,

$$\boldsymbol{F} \cdot \boldsymbol{F}^{\mathrm{p}} = \boldsymbol{F}^{\mathrm{e}} \cdot \boldsymbol{F}^{\mathrm{g}} \,. \tag{12}$$

This implies that the corresponding determinants,

$$\vartheta \;\; \vartheta^{\mathrm{p}} = \vartheta^{\mathrm{e}} \, \vartheta^{\mathrm{g}} \,, \tag{13}$$

are also multiplicatively related. In particular, ϑ represents the expansion-induced area change, ϑ^{p} is the area prestretch, ϑ^{e} is the reversible elastic area change, and ϑ^{g} is the permanently grown area change.

3. Results

The expansion of the left caudal region (P) was successfully completed. The expansion process spanned a total of six weeks with weekly filling volumes of 50 cc and three final days with an additional filling volume of 30 cc towards a total volume of 280 cc. The symmetric counterpart, the unexpanded right caudal region (Q), served as control. The expansion of the right rostral region (S) failed due to leakage of the inflation port and was not analyzed further. Figure 4 summarizes the four configurations of interest to characterize prestretch, expansion-induced deformation, and growth.

3.1. Characterization of prestretch

Figure 4, left, shows the kinematics associated with the prestretch $\boldsymbol{F}^{\mathrm{p}}$ as the mapping from the ex vivo to the in vivo configuration. We use the tattooed grid of the unexpanded right caudal region (Q) to quantify the regional variation of prestretch throughout the entire patch. Prestretch manifests itself as the tissue retraction upon explantation to reach a nearly stress free configuration.

Figure 5, left, summarizes the kinematics associated with prestretch. To re-establish the initial unit-square-sized skin patch with the tattooed grid of 10 cm × 10 cm, we would have to stretch the retracted ex vivo tissue patch by an average area prestretch of $\vartheta^{\mathrm{p}} = 1.44$. This corresponds to an area increase of 44% from the ex vivo to the in vivo configuration, or equivalently, to an area shrinkage of 31% upon explantation, corresponding to a retracted patch of 8.3 cm × 8.3 cm.

Figure 6 illustrates the characterization of prestretch using multi-view stereo and isogeometric analysis. The two columns show the skin patch in the ex vivo and in the prestretched in vivo configuration. The top row shows representative photographs of the experimental setup for each configuration. Using multi-view stereo, we create three-dimensional representations of the tattooed skin patch before the animal is sacrificed and after excising the patch. The middle row shows the geometric reconstruction of the skin patch. We choose the ex vivo pre-expansion state as reference configuration and the in vivo pre-expansion state as the current configuration. Using isogeometric analysis, we calculate the prestretch $\boldsymbol{F}^{\mathrm{p}}$ as the gradient of the mapping between both configurations. The associated area prestretch is $\vartheta^{\mathrm{p}} = \det(\boldsymbol{F}^{\mathrm{p}})$. The bottom row portrays the contour plot in the isogeometric parameter space.

Table 1: Characterization of average, maximum, and minimum area prestretch between the ex vivo pre-expansion and in vivo pre-expansion configurations.

area prestretch	$\vartheta^{\mathrm{p}}_{\mathrm{avg}}$ (-)	$\vartheta^{\mathrm{p}}_{\mathrm{max}}$ (-)	$\vartheta^{\mathrm{p}}_{\mathrm{min}}$ (-)	error (%)
ex vivo pre-expansion	1.00	1.00	1.00	13.1
in vivo pre-expansion	1.44	2.37	0.63	2.0

Table 1 summarizes the results of the prestretch analysis with an average area prestretch of $\vartheta^{\mathrm{p}}_{\mathrm{avg}} = 1.44$, a maximum area prestretch of $\vartheta^{\mathrm{p}}_{\mathrm{max}} = 2.37$, and a minimum area prestretch of $\vartheta^{\mathrm{p}}_{\mathrm{min}} = 0.63$. The geometric reconstruction error is 13.1% for the ex vivo configuration and 2.0% for the in vivo configuration.

3.2. Characterization of expansion-induced deformation

Figure 4, top right, shows the kinematics associated with the expansion-induced deformation $\boldsymbol{\varphi}$ and the deformation gradient $\boldsymbol{F}$ as the mapping from the in vivo pre-expansion configuration to the in vivo post-expansion configuration. We use the tattooed

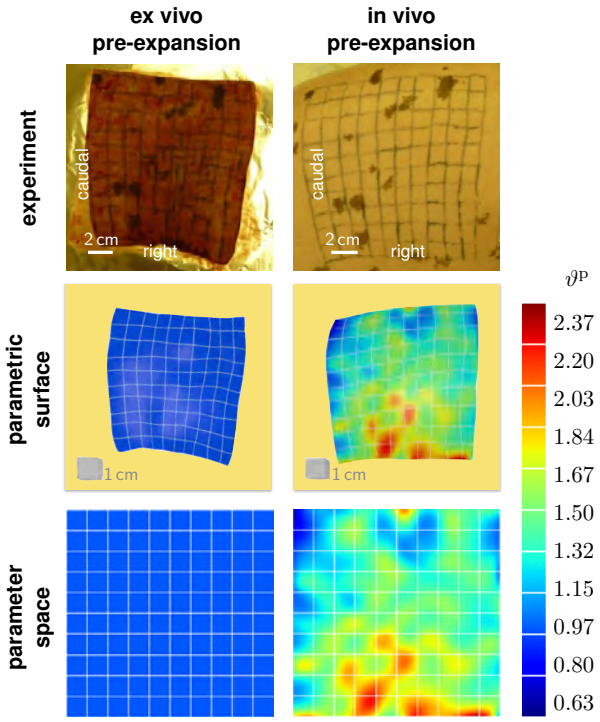

Figure 6: Characterization of prestretch using multi-view stereo and isogeometric analysis. Representative photographs of the experimental setup (top) enable reconstruction of the skin geometry using multi-view stereo (middle) to calculate the relative area change using isogeometric analysis (bottom). The area change between the ex vivo pre-expansion configuration (left) and the in vivo pre-expansion configuration (right) characterizes the amount of prestretch ϑ^{P}.

grid of the expanded left caudal region (P) to quantify the regional variation of the deformation throughout the entire patch.

Figure 5, top right, summarizes the kinematics associated with expansion-induced deformation. Within five weeks, the gradual expansion stretches the initial tattooed grid of 10 cm × 10 cm by $\vartheta = 1.87$. The surface area of the tattooed patch increases by 87%, which is the equivalent of a stretched patch with a side length of 13.7 cm × 13.7 cm.

Figure 7 illustrates the detailed time sequence of the expansion process. The top and bottom image sets show weekly photographs of the skin patch in vivo before and after the inflation step. Using multi-view stereo, we create a three-dimensional representation of each skin patch and compare it with the in vivo pre-expansion patch as reference configuration. Using isogeometric analysis, we calculate the deformation gradient $\boldsymbol{F}$ as the gradient of the mapping between both configurations and extract the total area change $\vartheta = \det(\boldsymbol{F})$. For each configuration, Figure 7 shows a photograph of the experimental setup, the B-spline surface color-coded with the area stretch ϑ, and the contour plot of ϑ in the isoparametric parameter space. The comparison from top to bottom characterizes the acute area stretch, imposed by abruptly filling the expander by 50 cc every week; the comparison from left to right characterizes the chronic area stretch, imposed by gradually increasing the filling volume to 280 cc. The contour plots reveal lower area stretches towards the beginning of the inflation process and higher area stretches towards the end. Changes in surface area displays drastic regional variations: Stretches are larger in the center of the expanded region and smaller in the periphery.

Table 2: Characterization of average, maximum, and minimum expansion-induced area stretch between the in vivo pre-expansion and in vivo post-expansion configurations. Throughout the five-week-long experiment, the expander volume increases weekly by 50 cc until it reaches its final value of 280 cc.

time (weeks)	volume (cc)	ϑ_{avg} (-)	ϑ_{max} (-)	ϑ_{min} (-)	error (%)
0^{pre}	0	1.00	1.00	1.00	4.7
0^{post}	50	1.17	2.49	0.41	0.9
1^{pre}	50	1.27	3.25	0.54	1.2
1^{post}	100	1.31	2.79	0.50	1.0
2^{pre}	100	1.38	2.86	0.37	0.9
2^{post}	150	1.43	3.21	0.33	1.0
3^{pre}	150	1.65	3.21	0.48	1.2
3^{post}	200	1.73	4.08	0.46	1.5
4^{pre}	200	1.73	3.50	0.36	1.2
4^{post}	250	1.77	3.52	0.48	1.2
5^{pre}	250	1.86	3.81	0.73	1.4
5^{post}	280	1.87	4.05	0.53	0.6

Table 2 summarizes time sequence of the expansion process throughout the five-week-long experiment. Triggered by the increase in expander volume, the average area stretch ϑ increases monotonically. At the end of week five, when the expander is filled to 280 cc, the average area stretch is $\vartheta_{\mathrm{avg}} = 1.87$, the maximum area stretch in the center region is $\vartheta_{\mathrm{max}} = 4.05$, and the minimum area stretch in the periphery is $\vartheta_{\mathrm{min}} = 0.53$. The geometric reconstruction error is largest for the initial configuration with a value of 4.7%, but takes values on the order of 1% for the remaining period of the experiment.

3.3. Characterization of growth

Figure 4, bottom, shows the kinematics associated with growth $\boldsymbol{F}^{\mathrm{g}}$ as the mapping from the ex vivo pre-expansion configuration to the ex vivo post-expansion configuration. Since we cannot compare the explanted ungrown and grown configurations of one and the same patch, we postulate that the dorsal midline acts as symmetry plane and assume that the amount of prestretch in the left caudal region (P) is equivalent to the amount of prestretch in the right caudal region (Q).

Figure 5, bottom, summarizes the kinematics associated with growth. To stretch the ex vivo post-expansion skin patch of average dimensions of 8.3 cm × 8.3 cm to the size of the explanted grown tissue patch of average dimensions of 12.5 cm × 12.5 cm, skin needs to grow by $\vartheta^{\mathrm{g}} = 2.25$. This corresponds to an area increase of 125% from the ex vivo pre-expansion to the ex vivo post-expansion skin patch. When compared to the in vivo post-expansion patch of average dimensions of 13.7 cm × 13.7 cm, the ex vivo post-expansion tissue patch shrinks by 17%, which corresponds to an elastic area stretch of $\vartheta^{\mathrm{e}} = 1.20$.

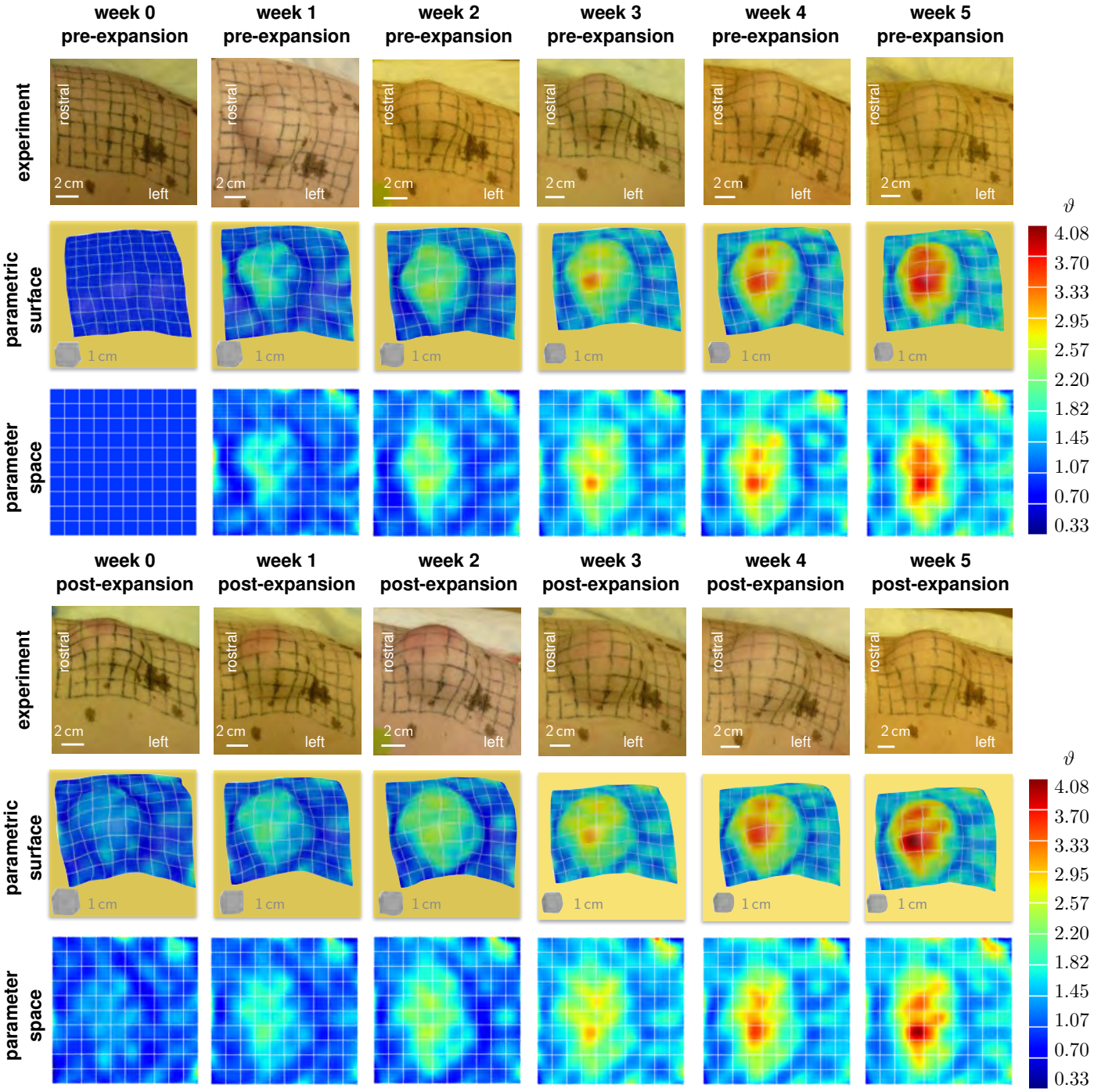

Figure 7: Characterization of expansion-induced area stretch using multi-view stereo and isogeometric analysis. The top and bottom image sets show the skin patch in the pre-expanded and post-expanded configuration. Representative photographs of the experimental setup (top) enable reconstruction of the skin geometry using multi-view stereo (middle) to calculate the area change using isogeometric analysis (bottom). Differences between the pre- and post-expansion characterize the acute stretch (top to bottom); differences between the post-expansion states characterize the chronic stretch (left to right).

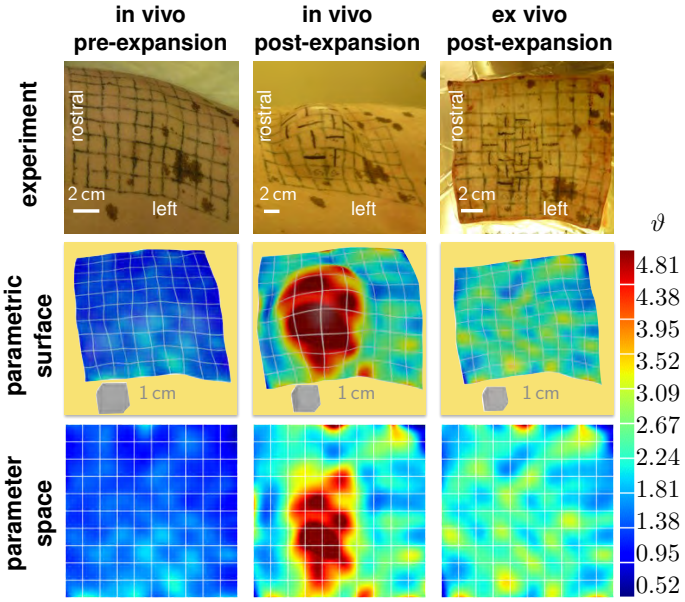

Figure 8: Characterization of growth using multi-view stereo and isogeometric analysis. Representative photographs of the experimental setup (top) enable reconstruction of the skin geometry using multi-view stereo (middle) to calculate the area change using isogeometric analysis (bottom). The area change in the in vivo pre-expansion configuration characterizes the amount of prestretch ϑ^{p} (left). The area change in the in vivo post-expansion configuration includes combined effects of prestretch and expansion-induced deformation $\vartheta\,\vartheta^{\mathrm{p}}$ (middle). The area change in the ex vivo post-expansion configuration characterizes the amount of growth ϑ^{g} (right).

Figure 8 illustrates the characterization of growth using multi-view stereo and isogeometric analysis. The first column shows the in vivo pre-expansion configuration with the build-in prestretch $\vartheta^{\mathrm{p}} = \det(\boldsymbol{F}^{\mathrm{p}})$. The second column showcases the in vivo post-expansion configuration, the physiological state after the expander has been filled to its full capacity, for which the area change is $\vartheta\,\vartheta^{\mathrm{p}} = \det(\boldsymbol{F} \cdot \boldsymbol{F}^{\mathrm{p}})$. The third column alludes to the ex vivo post-expansion configuration, which characterizes area growth as $\vartheta^{\mathrm{g}} = \det(\boldsymbol{F}^{\mathrm{g}})$. For each configuration in Figure 8 we show a representative photograph of the experimental setup, the isoparameteric surface reconstruction with the contour plot of the area change, and the contour plot in the isoparametric parameter space. The contour plots reveal that deformation-induced changes in surface area vary drastically across the tattooed patch: It appears that skin grows fastest in zones with highest overall deformation induced by expander inflation.

Table 3 summarizes the results of the total deformation analysis of combined prestretch and deformation and of the growth analysis. When compared to the ex vivo pre-expansion patch, the in vivo post-expansion patch has undergone a total area stretch of $(\vartheta\,\vartheta^{\mathrm{p}})_{\mathrm{avg}} = (\vartheta^{\mathrm{e}}\vartheta^{\mathrm{g}})_{\mathrm{avg}}$ =2.70, a maximum area stretch of $(\vartheta\,\vartheta^{\mathrm{p}})_{\mathrm{max}} = (\vartheta^{\mathrm{e}}\vartheta^{\mathrm{g}})_{\mathrm{max}}$ =6.99, and a minimum area stretch of $(\vartheta\,\vartheta^{\mathrm{p}})_{\mathrm{min}} = (\vartheta^{\mathrm{e}}\vartheta^{\mathrm{g}})_{\mathrm{min}} = 0.53$. When compared to the ex vivo pre-expansion patch, the ex vivo post-expansion patch has undergone an average area growth of $\vartheta^{\mathrm{g}}_{\mathrm{avg}}$=2.25, a maximum area growth of $\vartheta^{\mathrm{g}}_{\mathrm{max}} = 4.81$, and a minimum area growth of $\vartheta^{\mathrm{g}}_{\mathrm{min}} = 0.52$. i.e., the patch has more than doubled its initial area. The geometric reconstruction errors are 13.1%, 0.6%, and 1.7%.

Table 3: Characterization of average, maximum, and minimum area stretch between the ex vivo pre-expansion and in vivo post-expansion configurations and area growth between the ex vivo pre-expansion and ex vivo post-expansion configurations.

area stretch	$(\vartheta\,\vartheta^{\mathrm{p}})_{\mathrm{avg}}$ (-)	$(\vartheta\,\vartheta^{\mathrm{p}})_{\mathrm{max}}$ (-)	$(\vartheta\,\vartheta^{\mathrm{p}})_{\mathrm{min}}$ (-)	error (%)
ex vivo pre-expansion	1.00	1.00	1.00	13.1
in vivo post-expansion	2.70	6.99	0.53	0.6
area growth	$\vartheta^{\mathrm{g}}_{\mathrm{avg}}$ (-)	$\vartheta^{\mathrm{g}}_{\mathrm{max}}$ (-)	$\vartheta^{\mathrm{g}}_{\mathrm{min}}$ (-)	error (%)
ex vivo pre-expansion	1.00	1.00	1.00	13.1
ex vivo post-expansion	2.25	4.81	0.52	1.7

4. Discussion

We have designed and prototyped a novel experiment to quantitatively characterize the kinematics of living skin using multi-view stereo and isogeometric analysis. Our average geometric reconstruction error of 2.1% suggests that this method can serve as a easy-to-use yet highly accurate tool to reconstruct arbitrary three-dimensional surfaces.

Skin displays an incredible ability to adapt to mechanical cues from which we benefit in all day life during our development, growth, and wound healing. Understanding the biomechanics and mechanobiology of skin has received great attention: It can impact the design of medical devices, improve cosmetic products, and influence the outcomes of surgical procedures. Not surprisingly, intense research has been dedicated to characterize the mechanical properties of explanted, isolated specimens of skin. Yet, the mechanical characteristics of *living* skin in its natural environment remain poorly understood.

Here we perform controlled experiments of living skin to characterize prestretch, deformation, and growth in a porcine model of skin expansion. We take advantage of two recent trends in computer graphics: multi-view stereo and isogeometric analysis. Multi-view stereo is a technique to reconstruct of three-dimensional shapes from several two-dimensional images of the same scene. One of its major advantages is that it naturally captures physiologically relevant surface characteristics across the entire scene. Based on easy-to-create hand-held camera images, multi-view stereo is less expensive and more versatile than conventional, geometrically restrictive laboratory experiments. Isogeometric analysis allows us to use the resulting three-dimensional reconstructions to create smooth parametric surface representations. Isogeometric surfaces naturally satisfy the continuity requirements of thin membranes with relatively few arbitrary control points in space. To create a fixed set of control points, we tattooed a permanent grid onto the skin surface. This allows us to precisely quantify the relative deformation between different points in space and time and to identify regions of local extrema. Embedded into the framework of fictitious configurations, our isogeometric analysis naturally defines finite prestretch, deformation, and growth.

4.1. Skin prestretch

Our study shows that living skin is prestretched with an average area stretch of ϑ^{p}=1.44. The existence of prestretch in skin is in agreement with previous findings [29]. The amount of natural prestretch is also consistent, at least in magnitude, with experiments of human skin, which report an average prestretch of 1.57 in the forearm [19]. While prestretch has been widely characterized in arteries using opening angle experiments [20], disappointingly few studies address the natural tension in skin. Two recent studies have successfully identified prestrain [17] and initial stress [18] in human skin; however, both studies assume homogeneity of these fields. To our knowledge, our study is the first to characterize the regional distribution of prestretch across a sizable patch of skin. Our disproportionally large geometric reconstruction error is not inherently related to the characterization of prestretch; rather, it is caused by the small number of photographs, six as compared to at least ten for all other configurations. We are currently performing a follow-up study with an increased number of photographs, at least ten for all configurations, to eliminate this issue in the future. Naturally, an additional limitation is that the excised patch itself may still be under internal tension, which we could further release by cutting the patch into successively smaller pieces.

Prestretch has significant implications for our understanding of thin biological membranes [43]. Conceptually, prestretch is superposed to all in vivo deformation processes [2]. In the finite strain setting, this superposition is multiplicative - not just additive - which makes the inclusion of prestretch even more relevant: Prestretch shifts the stress-stretch curve to the left, here by a stretch of approximately -0.20 [17]. This implies that the characteristic strain stiffening associated with the untangling and stretching of collagen fibers takes place much earlier in vivo than predicted by ex vivo testing. Without including prestretch in the ex vivo test setup, the stiffness of skin is hugely overestimated. We have recently shown that the in vivo and ex vivo stiffnesses of biological membranes may differ by up to three orders of magnitude [42]. Our results support the hypothesis that prestretch is important to position thin biological membranes in vivo into their optimal operating range, right at the transition point of the exponential stiffening regime [43].

4.2. Skin deformation

Our study shows that living skin can be stretched locally by at least 4.05 in area without displaying signs of damage or rupture. This remarkable four-fold increase in area is made possible by gradually increasing the deformation over a period of several weeks. Specifically, our study reveals an average area stretch of 1.87 in response to a rectangular 4 cm $\times$ 6 cm tissue expander filled to 280 cc. This agrees well with reported values in the literature which range between 1.51 and 2.35 [56]. Several investigations have attempted to quantify the expansion process in the past [9]; however, most of them introduce restrictive approximations and their resolutions are coarse compared to ours. A unique feature of our method is the characterization of regional variations in area change using isogeometric analysis [11]. Our analysis confirms our common intuition that the deformation is not homogeneous across the expanded area: The area change is largest in the center of the expanded region and decays gradually towards the edges of the skin patch. This agrees excellently with our computational simulations of skin growth, which predict a four-fold local area increase in the center region and gradual decay towards the periphery [10].

4.3. Skin growth

Our study shows that skin responds to chronic overstretch by growing in area, in our specific case by a factor 2.25. This implies that the skin patch more than doubled its initial area within a period of five weeks. Using a symmetric control patch from the same animal, we were able to quantify, for the first time, the amount of skin growth with respect to the stress free ex vivo configuration. We observe that the total area increase of 2.70, which is a result of combined prestretch of 1.44 and expander-induced deformation of 1.87, reflects the combined effects of a reversible elastic stretch of 1.20 and permanent growth of 2.25. Our contour plots display a regional variation of growth with local maxima of 4.81, a four-fold increase in area around the center region, and local minimal of 0.52, a decrease in area around the periphery. This is in excellent agreement with previous experimental measurements [6] and computational predictions [10]. It appears that, in general, regions with large overall deformation also exhibit large growth [57]. However, regions with extreme deformation do display large but not extreme growth. These observations provoke two speculations: First, growth seems to be triggered by chronic mechanical overstretch. Second, the amount of growth seems to be limited by the rate at which new skin can be created. Accordingly, zones with extreme overall deformation may not exhibit extreme growth. A potential limitation is obviously that we only examine the animal for five weeks and do not follow it long-term.

Growth has important implications for various clinical procedures in plastic and reconstructive surgery [34]. Recent studies have used computational models to predict skin growth in response to mechanical loading [10, 50]. Experimental data to calibrate these models exist [6], yet, at a very low spatial and temporal resolution. With 11×11 points in space and 12 points in time, our study is the first to quantify area growth in skin at a high spatial and temporal resolution. More importantly, our method allows us to non-invasively reconstruct the in vivo pre-expansion, in vivo post-expansion, and ex vivo post-expansion configurations and the corresponding mappings $\boldsymbol{F}$, $\boldsymbol{F}^{\mathrm{e}-1} \cdot \boldsymbol{F}$, and $\boldsymbol{F}^{\mathrm{e}}$ from simple hand-held camera images [24]. As such, our approach is less expensive and more flexible than standard laboratory techniques. With the exception of prestrain, our method can be easily adopted in a clinical setting to characterize the in vivo kinematics of living skin during long-term procedures such as tissue expansion [23].

4.4. Limitations

Our experimental setup has a few additional limitations: First, as a proof of concept, this study is based on a single animal, which does not allow us to make statistical statements

about the growth process. Second, throughout the six-week long study, the animal itself undergoes natural growth, an effect which we consider secondary in the present work, but which we could easily eliminate using the geometries of the non-expanded control patch. Third, our isogeometric analysis relies on following material points from one time point to the next; here, these are the 11×11 nodes of the tattooed grid. This may be too coarse for an accurate interpolation, in particular in the analysis of prestretch for which finer grids and a successive subdivision of the explanted patch would be desirable. Fourth, as a first step, we have only considered the area change in skin, while it would be desirable to separately characterize the kinematic changes along and perpendicular to the directions of tissue anisotropy. Fifth, a longitudinal study with multiple time points of tissue harvest would be desirable to truly quantify the speed of growth. Sixth, while the in vivo pre-expansion, in vivo post-expansion, and ex vivo post-expansion configurations can be extracted non-invasively in any human tissue expansion procedure, the ex vivo pre-expansion configuration requires the invasive explantation of an intact tissue patch and should only be used for initial baseline calibrations of prestretch. Finally, an obvious additional limitation is the related to generalizing our findings from animals to human.

5. Concluding remarks

We have presented a novel, simple and inexpensive approach towards characterizing the mechanics of thin biological membranes in their natural in vivo environment. Our method combines multi-view stereo and isogeometric analysis to quantify the kinematics of living skin. We illustrate our approach by means of a porcine model of skin expansion to explore the key aspects of prestretch, deformation, and growth. Globally, our method reveals an average area prestretch of 1.44, an average area stretch of 1.87 after five weeks of expansion, and an average area growth of 2.25. Beyond quantifying these average global quantities, our method is inherently designed to characterize local variations and identify regions of extreme deformation. Locally, our analysis reveals a maximum prestretch of 2.37 in the ventral region, a maximum expansion-induced area stretch of 4.05 in the center region of the expander, and a maximum area growth of 4.81 in the region of maximum stretch. The next logical step would be to identify the underlying biochemical mechanisms of prestretch, deformation, and growth and correlate them to our kinematic measurements. Our study has immediate impact on understanding living skin to optimize treatment planning and establish predictive tools to guide surgical decision making. Our experimental design has broad applications beyond skin expansion: It provides a flexible, robust, low cost, easy-to-use tool for the surface reconstruction of living membranes, which are difficult to characterize in a conventional laboratory setup.

Acknowledgements

This work was supported by the CONACyT Fellowship and by the Stanford Graduate Fellowship to Adrian Buganza Tepole and by the National Science Foundation CAREER award CMMI 0952021, by the National Science Foundation INSPIRE grant 1233054, and by the National Institutes of Health Grant U54GM072970 to Ellen Kuhl.

References

[1] Ambrosi D, Ateshian GA, Arruda EM, Cowin SC, Dumais J, Goriely A, Holzapfel GA, Humphrey JD, Kemkemer R, Kuhl E, Olberding JE, Taber LA, Garikipati K. Perspectives on biological growth and remodeling. *J Mech Phys Solids*. 2011;59:863-883.

[2] Amini R, Eckert CE, Koomalsingh K, McGarvey J, Minakawa M, Gorman JH, Gorman RC, Sacks MS. On the in vivo deformation of the mitral valve anterior leaflet: Effects of annular geometry and referential configuration. *Ann Biomed Eng.* 2012;40:1455-1467.

[3] Austad ED, Pasyk KA, McClatchey KD, Cheery GW. Histomorphologic evaluation of guinea pig skin and soft tissue after controlled tissue expansion. *Plast Reconstr Surg.* 1982;70:704-710.

[4] Badir S, Bajka M, Mazza E. A novel procedure for the mechanical characterization of the uterine cervix during pregnancy. *J Mech Beh Biomed Mat.* 2013;27:143-153.

[5] Bartell TH and Mustoe TA. Animal models of human tissue expansion. *Plast Reconstr Surg.* 1989;83:681-686.

[6] Beauchenne JG, Chambers MM, Peterson AE, Scott PG. Biochemical, biomechanical, and physical changes in the skin in an experimental animal model of therapeutic tissue expansion. *J Surg Res*. 1989;47:507-514.

[7] Benson DJ, Bazilevs Y, Hsu MC and Hughes TJR. Isogeometric shell analysis: the Reissner-Mindlin shell. *Comput Method Appl Mech Eng.* 2010;199:276-289.

[8] Böl M, Ehret AE, Leichsenring K, Weichert C, Kruse R. On the anisotropy of skeletal muscle tissue under compression. *Acta Biomat.* 2014; doi:10.1016/j.actbio.2014.03.003.

[9] Brobmann GF and Huber J. Effects of different-shaped tissue expanders on transluminal pressure, oxygen tension, histopathologic changes, and skin expansion in pigs. *Plast Reconstr Surg.* 1985;76:731-736.

[10] Buganza Tepole A, Ploch CJ, Wong J, Gosain AK, Kuhl E. Growin skin: A computational model for skin expansion in reconstructive surgery. *J Mech Phys Solids.* 2011;59:2177-2190.

[11] Buganza Tepole A, Gosain AK, Kuhl E. Stretching skin: The physiological limit and beyond. *Int J Nonlin Mech.* 2012;47:938-949.

[12] Buganza Tepole A, Kuhl E. Review: Systems-based approaches towards wound healing. *Pediatric Res.* 2013;73:553-563.

[13] Buganza Tepole A, Steinberg JP, Kuhl E, Gosain AK. Application of finite element modeling to optimize flap design with tissue expansion. *Plast Reconstr Surgery.* 2014; in press.

[14] Cottrell JA, Hughes TJ and Bazilevs Y. Isogeometric analysis: toward integration of CAD and FEA. John Wiley & Sons. 2009.

[15] De Filippo RE, Atala A. Stretch and growth: the molecular and physiologic influences of tissue expansion. *Plast Reconstr Surg.* 2002;109:2450-2462.

[16] Echter R, Oesterle B, Bischoff M. A hierarchic family of isogeometric shell finite elements. *Comput Method Appl Mech Eng.* 2013;254:170-180.

[17] Evans SL, Hold CA. Measuring the mechanical properties of human skin in vivo using digital image correlation and finite element modelling. *J Strain Anal Eng Design.* 2009;44:337-345.

[18] Flynn C, Taberner A, Nielsen P. Mechanical characterisation of in vivo human skin using a 3D force-sensitive micro-robot and finite element analysis. *Biomech Model Mechanobiol.* 2011;10:27-38.

[19] Flynn C, Taberner A, Nielsen P. Modeling the mechanical response of in vivo human skin under a rich set of deformations. *Ann Biomed Eng.* 2011;39:1935-1946.

[20] Fung, YC. What are the residual stresses doing in our blood vessels? *Ann Biomed Eng.* 19:237-249,1991.

[21] Furukawa Y, Ponce J. Accurate, dense, and robust multi view stereopsis. *IEEE T Pattern Anal.* 2010;32:1362-1376.

[22] Geerligs M, van Breemen L, Peters G, Ackermans P, Baaijens F, Oomens C. In vitro indentation to determine the mechanical properties of epidermis. *J Biomech.* 2011;44:1176-1181.

[23] Gosain AK, Zochowski CG, Cortes W. Refinements of tissue expansion

for pediatric forehead reconstruction: A 13-year experience. *Plast Reconstr Surg.* 2009;124:1559-1570.
[24] Hiep V, Keriven P, Labatut P and Pons JP. Towards high-resolution large-scale multi view stereo. *IEEE Conference on CVPR.* 2009.
[25] Holzapfel GA. Large strain analysis of soft biological membranes: Formulation and finite element analysis. *Comp Meth App Mech Eng.* 1996;132:45-61.
[26] Hughes, TJ. The finite element method: Linear static and dynamic finite element analysis. Prentice Hall Inc. Englewood Cliffs, NJ. 1987.
[27] Hughes TJ, Cottrell JA and Bazilevs Y. Isogeometric analysis: CAD, finite elements, NURBS, exact geometry and mesh refinement. *Comput Method Appl Mech.* 2005;194:4135-4195.
[28] Humphrey JD. Review Paper: Continuum biomechanics of soft biological tissues *Proc R Soc Lond A.* 2003;459:3-46.
[29] Jor JWY, Nash MP, Nielsen PMF and Hunter PJ. Estimating material parameters of a structurally based constitutive relation for skin mechanics. *Biomech Model Mechanobiol.* 2011;10:767-778.
[30] Kiendl J, Bletzinger KU, Linhard J, and Wüchner R. Isogeometric shell analysis with Kirchhoff-Love elements. *Comput Method Appl Mech Eng.* 2009;198:3902-3914.
[31] Lamers E, van Kempen THS, Baaijens FPT, Peters GWM, Oomens CWJ. Large amplitude oscillatory shear properties of human skin. *J Mech Beh Biomed Mat.* 2013;28:462-470.
[32] Lanir Y, Fung YC. Two-dimensional mechanical properties of rabbit skin - I. Experimental system. *J Biomech.* 1974;7:29-34.
[33] Limbert G, Simms C. Special issue on skin mechanobiology. *J Mech Beh Biomed Mat.* 2013;28:395-396.
[34] LoGiudice J, Gosain AK. Pediatric tissue expansion: Indications and complications. *J Craniofac Surg.* 2003;14:866-872.
[35] Lhuillier M, Quan L. A quasi-dense approach to surface reconstruction from uncalibrated images. *IEEE T Pattern Anal* 2005;27:418-433.
[36] Mazza E, Nava A, Bauer M, Winter R, Bajka M, Holzapfel GA. Mechanical properties of the human uterine cervix: An in vivo study. *Med Im Anal.* 2006;125-136.
[37] Meyer W, Schwarz R, Neurand K. The skin of domestic mammals as a model for the human skin, with special reference to the domestic pig. *Curr Probl Dermatol.* 1978;7:39-52.
[38] Montagna W, Yun JS. The skin of the domestic pig. *J Invest Dermatol.* 1964;42:11-21.
[39] Myers KM, Coudrillier B, Boyce BL, Nguyen TD. The inflation response of the posterior bovine sclera. *Acta Biomat.* 2010;6:4327-4335.
[40] Pailler-Mattei C, Bec S, Zahouani H. In vivo measurements of the elastic mechanical properties of human skin by indentation tests. *Med Eng Phys.* 2008;30:599-606.
[41] Rausch MK, Bothe W, Kvitting JP, Gktepe S, Miller DC, Kuhl E. In vivo dynamic strains of the ovine anterior mitral valve leaflet. *J Biomechanics.* 2011;44:1149-1157.
[42] Rausch MK, Famaey N, O'Brien Shultz T, Bothe W, Miller DC, Kuhl E. Mechanics of the mitral valve: A critical review, an in vivo parameter identification, and the effect of prestrain. *Biomech Model Mechanobiol.* 2013;12:1053-1071.
[43] Rausch MK, Kuhl E. On the effect of prestrain and residual stress in thin biological membranes. *J Mech Phys Solids.* 2013;61:1955-1969.
[44] Rausch MK, Kuhl E. On the mechanics of growing thin biological membranes. *J Mech Phys Solids.* 2014;63:128-140.
[45] Rodriguez EK, Hoger A, McCulloch AD. Stress-dependent finite growth in soft elastic tissues. *J Biomech.* 1994;27:455-467.
[46] Seitz SM, Curless B, Diebel J, Scharstein D, Szeliski R. A comparison and evaluation of multi-view stereo reconstruction algorithms. *IEEE Conference on Computer Vision and Pattern Recognition.* 2006;1:519-528.
[47] Shively RE. Skin expander volume estimator. *Plast Reconstr Surg.* 1986;77:482-483.
[48] Silver FH, Siperko LM, Seehra GP. Mechanobiology of force transduction in dermal tissue. *Skin Res Tech.* 2003;9:3-23.
[49] Slabaugh G, Culbertson B. A survey of methods for volumetric scene reconstruction from photographs. *VG'01 Proceedings of the 2001 Eurographics Conference on Volume Graphics.* 2001;81-101.
[50] Socci L, Pennati G, Gervaso F, Vena P. An axisymmetric computational model of skin expansion and growth. *Biomech Model Mechanobiol.* 2007;6:177188.
[51] Stretcha C, von Hansen W, Van Gool L, Fua P, Thoennessen U. On benchmarking camera calibration and multi view stereo for high resolution imagery. *IEEE Conference on CVPR.* 2008.
[52] Sullivan TP, Eaglstein WH, Davis SC, Mertz P. The pig as a model for human wound healing. *Wound Repair Regen.* 2001;9:66-76.
[53] Tong P, Fung YC. The stress-strain relationship for the skin. *J Biomech.* 1976;9:649-657.
[54] Tonge TK, Atlan LS, Voo LM, Nguyen TD. Full-field bulge test for planar anisotropic tissues: Part I - Experimental methods applied to human skin tissue. *Acta Biomat.* 2013;9:5913-5925.
[55] Tonge TK, Voo LM, Nguyen TD. Full-field bulge test for planar anisotropic tissues: Part II - A think shell method for determining material parameters and comparison of two distributed fiber modeling approaches. *Acta Biomat.* 2013;9:5926-5942.
[56] van Rappard JHA, Molenaar J, van Doorn K, Sonneveld GJ, Borghouts JMHM. Surface-area increase in tissue expansion. *Plast Reconstr Surg.* 1988;82:833-839.
[57] Zöllner AM, Buganza Tepole A, Kuhl E. On the biomechanics and mechanobiology of growing skin. *J Theor Bio.* 2012;297:166-175.
[58] Zöllner AM, Buganza Tepole A, Gosain AK, Kuhl E. Growing skin - Tissue expansion in pediatric forehead reconstruction. *Biomech Model Mechanobiol.* 2012;11:855-867.
[59] Zöllner AM, Holland MA, Honda KS, Gosain AK, and Kuhl E. Growth on demand: Reviewing the mechanobiology of stretched skin. *J Mech Beh Biomed Mat.* 2013;28:495-509.